nature communications

Article

https://doi.org/10.1038/s41467-025-62075-4

Nucleophilic addition promoted ring rearrangement-aromatization in aza-/thio-sesquiterpenoid biosynthesis

Received: 18 January 2025

Accepted: 10 July 2025

Published online: 09 August 2025

Check for updates

Hengyi Xu[1,2], Xianyan Zhang[1], Yawen Zhang[1], Guowei Liu[1], Yinghan Chen[1,3], Xuewen Hou[1,2], Xiaolin Liu[1,2], Kaijin Zhang[1], Chuanteng Ma[1], Ruqian Feng[4], Juan Shen[4], Blaine A. Pfeifer[5], Qian Che[1], Tianjiao Zhu[1] & Guojian Zhang[1,2,6]

The aromatization of terpenoid scaffold has received enduring attention as it introduces diverse structural alterations and endows bioactivity to the molecules. In this study, we discover a unique aromatization mechanism involving consecutive [1,2]-alkyl migrations initiated by intramolecular oxa/aza-nucleophilic addition in the biosynthesis of a family of eremophilane-like sesquiterpenoid derivatives, including farfugin A (**1**) and aza-janthinellin A (**2a**), a sesquiterpene-amino acid adduct. During this process, JanF, a flavoprotein functioning as a dehydrogenase, is demonstrated to be able to oxidize an allyl alcohol group of eremophilanes into an α,β-unsaturated aldehyde, thereby facilitating the binding of primary amines to the sesquiterpene skeleton. Furthermore, using JanF as a catalyst, we generate a series of aromatic aza-/thio-sesquiterpenoids (aza-janthinellins and thio-janthinellins), among which, thio-janthinellins exhibit potent cytotoxicity against human chronic myelogenous leukemia K562 cells. These findings advance our understanding of the biogenesis of aromatic compounds and enable the construction of diverse aza-/thio-terpenoids with enhanced biological activity.

Aromatization is a critical process in the biosynthesis of natural products (NPs) and influences various metabolic pathways. In the shikimate pathway, the aromatization of the key intermediate in chorismic acid metabolism gives rise to the aromatic amino acids and other benzene derivatives, including phenolic acids and phenylpropanoids[1]. In the type II polyketide biosynthetic pathway, aldol condensation initiates aromatization of the non-reducing polyketide precursor, leading to the formation of aromatic clinical pharmaceuticals such as doxorubicin and tetracycline[2,3].

In addition to the above cases, there are some other distinct origins of aromatic rings, such as in terpene biosynthesis, during which aromatization of the poly-isoprenoid scaffold may occur and be mediated by specific tailoring enzymes to generate unique aromatic terpenoids. For example, the sequential dehydrations of a dihydroxy-keto intermediate catalyzed by a specialized ubiquitous glyoxalase (SPG) led to the formation of the partially aromatized product of furocalamen (Fig. 1A, i), which is the key intermediate of gossypol, a well-known chemical defense compound in cotton plants (*Gossypium*

[1]Key Laboratory of Marine Drugs, Chinese Ministry of Education, School of Medicine and Pharmacy, Ocean University of China, Qingdao 266003, China. [2]Laboratory for Marine Drugs and Bioproducts, Qingdao Marine Science and Technology Center, Qingdao 266237, China. [3]State Key Laboratory of Coordination Chemistry, Jiangsu Key Laboratory of Advanced Organic Materials, Chemistry and Bio-medicine Innovation Center, School of Chemistry and Chemical Engineering, Nanjing University Nanjing 210023, China. [4]Guangdong Provincial Key Laboratory of Pharmaceutical Bioactive Substances, Guangdong Pharmaceutical University, Guangzhou 510006, China. [5]Department of Chemical and Biological Engineering, University at Buffalo, The State University of New York, Buffalo, NY 14260, USA. [6]Marine Biomedical Research Institute of Qingdao, Qingdao 266101, China. e-mail: zhangguojian@ouc.edu.cn

https://doi.org/10.1038/s41467-025-62075-4

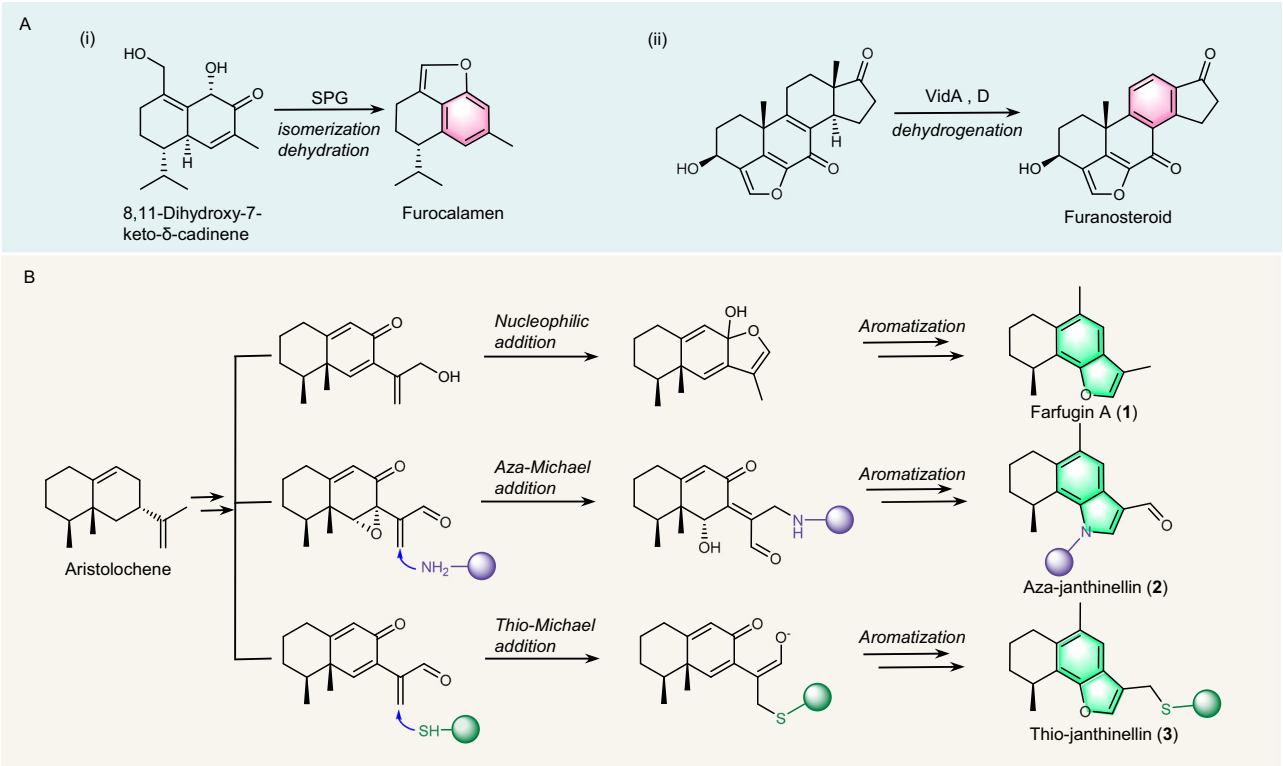

Fig. 1 | Representatives of terpenoid aromatization. A Aromatization of the intermediate of gossypol by SPG (i). The formation of aromatic furanosteroid catalyzed by two P450s, VidA, D (ii). **B** Generation of aromatic eremophilenes (this work).

spp.)[4]. The sequential dehydrogenations catalyzed by two P450 enzymes in furanosteroid biosynthesis resulted in the aromatization of the steroid skeleton (Fig. 1A, ii)[5].

Eremophilanes represent a prominent class of sesquiterpenoids, distinguished by diverse skeletal structures and notable bioactivities with potential medicinal applications[6,7]. Examples include the RNA polymerase inhibitor PR-toxin[8] and the cytotoxic agent 3-acetyl-13-deoxyphomenone (Fig. S1)[9]. Biogenetically, all eremophilanes originated from the aristolochene framework, which is a typical sesquiterpenoid synthesized through cyclization of farnesyl diphosphate (FPP) catalyzed by aristolochene synthetase (AS, a terpene cyclase)[10,11]. Unlike canonical sesquiterpenes, the family of eremophilanes-type terpenoids is comprised of a group of aromatic structures, for example, paraconiothin H from *Paraconiothyrium brasiliense*[12], citreobenzofuran D from *Penicillium janthinellum*[13], and farfugin A (**1**) from *Farfugium japonicum*[14] (Figure S1). Distinct from those as thus far documented aromatization processes for the formation of furocalamen and furanosteroid[4,5], the formation of the above aromatic eremophilanes-type terpenoids involves disruption and rearrangement of the poly-isoprenoid framework, generating skeletons with a structurally close resemblance to aromatic polyketides. This previously unrecognized aromatization process implied in eremophilanes biosynthesis has prompted our interest in further investigation.

In our recent work within the scope of natural product discovery assisted by genome mining tools, we identified a silent sesquiterpenoids biosynthetic gene cluster (BGC, *jan* cluster) from a fungal strain of *Penicillium janthinellum* H7-4 (Fig. S2). The cluster was activated by overexpressing a pathway-specific transcriptional factor (JanG), and resulted in the production of the non-aromatic eremophilane derivative of phomenone B (**6**)[13] and the aromatic structure of farfugin A (**1**)[14] (Fig. S2). Further heterologous expression of the functional genes (*jan*ABCDEF) in *Aspergillus nidulans* A1145 afforded a variety of diversified eremophilanes, including compound **1** and an aromatic sesquiterpenoid-amino acid adduct of aza-janthinellin A (**2a**) (Fig. 1B), accompanied by several non-aromatic structures like phomenonol A (**7**), which showed promising anti-inflammatory activity. Of interest, **2a** possesses an unusual aza-aromatic terpenoid skeleton derived from the integration of a sesquiterpene with L-threonine. Subsequent biosynthetic studies demonstrated a unique aromatization mechanism involving the rearrangement of the cyclohexenone skeleton, initiated by nucleophilic addition and consecutive [1,2]-alkyl migrations in the assembly line of **1** and **2a**. During this process, a FAD-dependent monooxygenase (FMO), JanF, is identified to be indispensable for the formation of the aza-janthinellin structures by catalyzing the oxidation of the allyl alcohol end group into an α,β-unsaturated aldehyde, which serves as a highly reactive intermediate undergoing nucleophilic attack. Moreover, JanF also proves to be able to selectively direct the 1,2-addition reaction of the α,β-unsaturated ketone structure, which is the critical step in generating the partial aromatic skeleton. Further promiscuity studies on JanF led to the production of a series of alkyl thiols-coupled aromatic sesquiterpenoids named as thio-janthinellins (**3**) (Fig. 1B).

Here in this report, we describe the discovery the aromatic eremophilane-like sesquiterpenoids, including farfugin A and aza-janthinellin A, the formation of farfugin A and aza-janthinellin A, which involves ring arrangement and aromatization initiated by heteroatom nucleophilic addition, and the dehydrogenation function of the FAD-dependent monooxygenase JanF in mediating the aromatization process of the sesquiterpenoid skeleton.

Results

Identification of the *Jan* BGC

The mangrove endophytic fungus *P. janthinellum* H7-4 was sequenced, and the genomic data were mined by scanning the DNA sequences using *prx-ORF2*[15], an aristolochene synthetase (AS, a terpene cyclase) responsible for the biosynthesis of eremophilanes, as a probe. As a result, we located a biosynthetic gene cluster (BGC) named *jan*, which spans approximately 16.5 kb, comprising eight genes. Along with the

https://doi.org/10.1038/s41467-025-62075-4

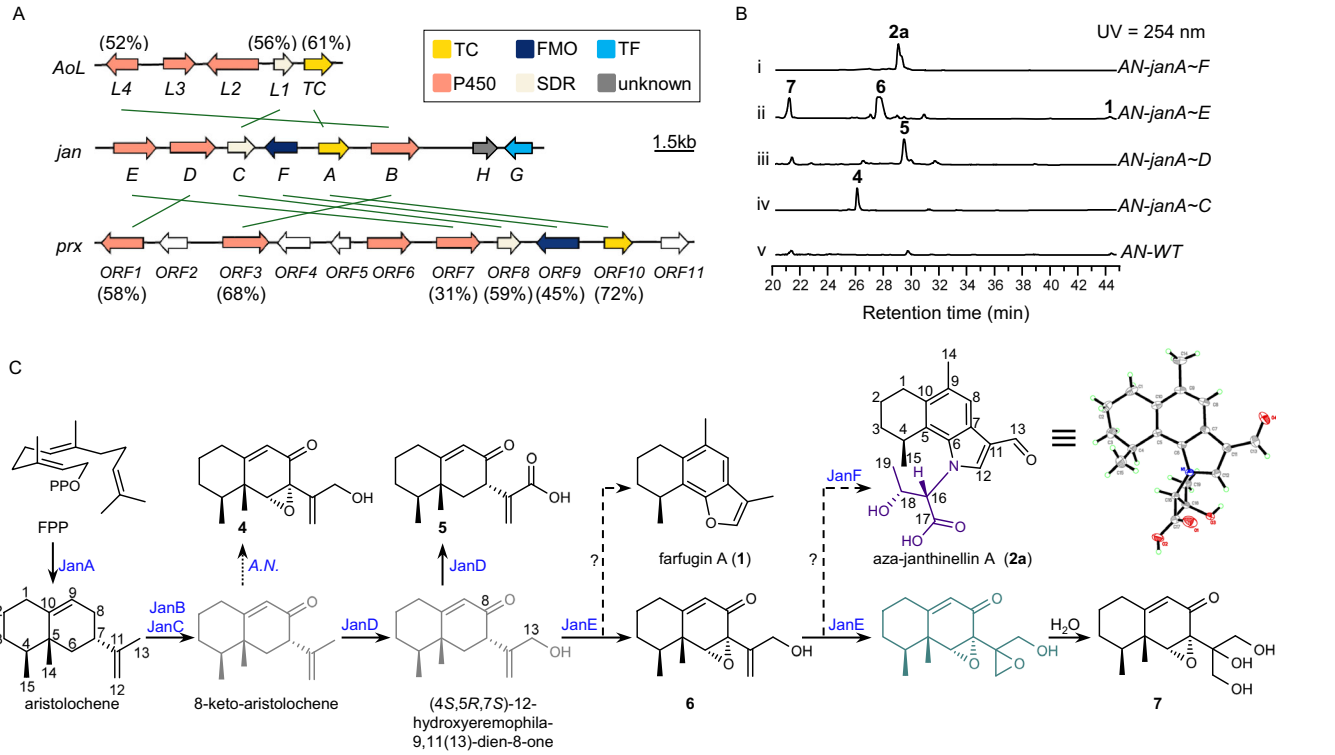

Fig. 2 | Identification of *jan* gene cluster governing the biosynthesis of farfugin A (1) and janthinelin A (2a). A Comparison of the *jan* gene cluster in *Penicillium janthinellum* H7-4 with the *AoL* cluster and the *prx* cluster. **B** HPLC analysis of metabolites produced by stepwise heterologous expression of *jan* genes in *Aspergillus nidulans*. **C** Proposed biosynthetic pathway of farfugin A (**1**) and janthinelin A (**2a**).

characteristic terpene cyclase of AS (JanA), seven neighboring and tailoring genes (JanB-H) were identified, encoding three cytochrome P450 enzymes (JanB, D, E), a short-chain dehydrogenase (JanC), a FAD-dependent monooxygenase (JanF), a pathway-specific transcriptional factor (JanG), and an unknown protein (JanH) (Fig. 2A, Table S1). This *jan* cluster shows homology with the previously reported gene clusters of *AoL*, which produces the compound 2-hydroxy, 8-oxo-aristolochene[16] and *prx*, which is responsible for the production of PR-toxin[10,11] (Fig. 2A). The above information suggests the capacity of the *jan* cluster to produce versatile aristolochene-like sesquiterpenoids; however, as indicated by the transcriptomic data and metabolic profile, the *jan* cluster remains silent or unexpressed in the wild type of H7-4 (Fig. S2B). We then activated the *jan* cluster by overexpressing JanG, a zinc finger protein designated as a pathway-specific regulatory transcriptional factor (Fig. S2C). The mutant strain with the overexpression of JanG successfully produced phomenone B (**6**)[13] (Fig. S2A), a canonical eremophilane derivative with a non-aromatic skeleton and compound **1**, with the intriguing aromatic structure (Figs. S2A, S27-S28, CCDC 2341506, and Table S5).

Reconstitution of the *Jan* Cluster in *A. nidulans* resulted in the production of aromatic sesquiterpenoids of farfugin A (1) and aza-janthinellin A (2a)

To better understand the logic of the biosynthetic assembly line encoded by the *jan* gene cluster, especially the biosynthetic steps of the aromatic sesquiterpenoids, we then conducted stepwise reconstitution of the *jan* genes in the filamentous model strain of *A. nidulans* A1145. Protein sequence alignment showed that JanA-C have high amino acid identity with AoTC, AoL4, and AoL1, which are involved in the PR-toxin biosynthetic pathway of 8-keto-aristolochene (Fig. 2A)[16]. Based on this analysis, the biosynthetic genes *janA ~ C* were cloned from the genome of H7-4 and heterologously expressed in the fungal host *A. nidulans* A1145 (Fig. 2B, iv)[17], which resulted in the production of 3-hydroxy-8-oxo-aristolochene (**4**, Figs. S169–S170, and Table S8)[18]. This result was consistent with the reported functions of JanB-C as cytochrome P450 enzymes that cooperatively introduce the C-8 carbonyl group[16]. The extra P450 enzyme gene *janD* was then co-expressed with *janA ~ C*, leading to the production of the 13-carboxyl congener of **5** (Figs. S171–S172, and Table S8)[16], which confirmed for the first time that JanD is responsible for oxidation at the C-13 position (Fig. 2B, iii). Subsequently, co-expression of *janA ~ E* resulted in the generation of three metabolites: phomenone B (**6**, Figs. S173–S174, and Table S9)[13], phomenonol A, a new structure resulting from the ring-opening of the epoxide at C11–12 in **6** (**7**, Fig. 2C, Figs. S175–S181, and Table S10), and the aromatic structure of farfugin A (**1**) (Fig. 2B, ii). Then, the gene *janF* was added to the *AN-janA ~ E* cotransformant (Fig. 2B, i), leading to the depletion of compounds **1, 6**, and **7**, but accumulation of aza-janthinellins A (**2a**, Figs. S36–S42, and Table S6), which was identified as a novel structure featuring an aromatic sesquiterpene skeleton covalently bonded to L-threonine. The stereochemical configuration of **2a** was further determined by Marfey's method (Fig. S3), ECD calculation (Fig. S26), and single-crystal X-ray analysis (CCDC 2341504, Fig. 2C). Notably, compound **2a** represents the Initial example of a naturally occurring terpenoid featuring a cyclohexyl-fused indole skeleton derived from an azaphilic process.

These results give a general sketch of the biosynthetic pathway leading to the aromatic eremophilanes: the common precursor of FPP was cyclized by JanA to give the aristolochene skeleton, which was then processed by JanB-D to afford (4*S*,5*R*,7*S*)-12-hydroxyeremophila-9,11(13)-dien-8-one (Fig. 2C)[19]. This previously reported non-aromatic eremophilane could be oxidized by JanE to generate the epoxide derivatives of **6** and **7** (Fig. 2C). However, the generation of the aromatic structures of **1** and **2a**, with the catalysis of JanE and JanF, remained a mystery that needed to be solved.

https://doi.org/10.1038/s41467-025-62075-4

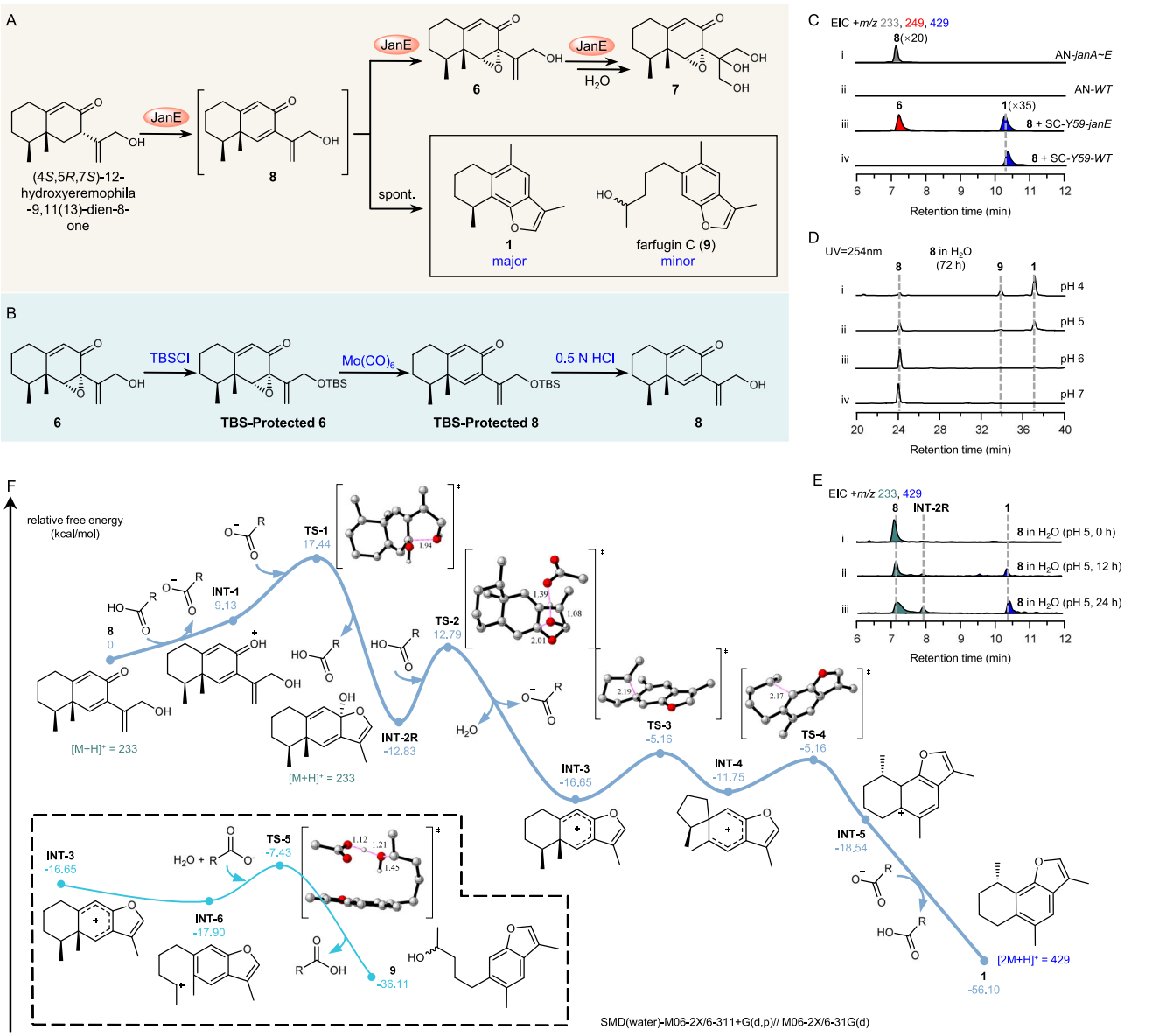

Fig. 3 | Detailed studies on the enzymatic and non-enzymatic transformation of 8. A The biosynthetic routes of the enzymatic and spontaneous transformation of **8**. **B** The chemical synthesis converting **6** into **8**. **C** LC–MS analysis of in vivo biotransformation in *A. nidulans* and *S. cerevisiae* demonstrated JanE is responsible for the formation of **6** from **8** but not involved in the formation of **1**. **D** HPLC analysis of spontaneous reactions of **8** at 30 °C for 72 h in H_2O. **E** LC–MS analysis of **INT-2R** during the acid-mediated conversion of compound **8** to **1** in citric acid/Na_2HPO_4 buffer (pH 5). **F** DFT calculations for the process of [1,2]-methyl migrations from **8** to **1** and **9** (Cartesian coordinates of the optimized structure shown in Supplementary Data 1).

The formation of farfugin A (1) involves the rearrangement of the cyclohexenone skeleton

Recently, it has been proposed that the formation of aromatic eremophilanes like paraconiothins *H–J* involves carbocation rearrangement following the initial eremophilane skeleton construction (Fig. S4)[12]. This hypothesis still requires rigorous experimental validation. To test the production of compound **1**, we fed two non-aromatic structures of **6** and **7**, which were co-discovered along with **1** by heterologous expression of *janA ~ E*, into the culture of the strain *AN-janB ~ E*. However, **1** was not detected from the fermentation products by LC-MS (Fig. S5), indicating that compound **6** or **7** is unlikely to be the precursor leading to **1**. We then imagined there might be some product upstream of **6** and **7** serving as the precursor of **1**. This speculation was emphasized by the detection of an ion peak (compound **8**, m/z 233 $[M+H]^+$) with trace amounts in the LC–MS profile of the *AN-janA ~ E* cotransformant (Fig. 3C, i). Meanwhile, recent reports indicated that the C6–7 epoxide product could be transformed from its olefinic precursor under the catalysis of Aoy13, a homology of P450 enzyme JanE functioning in eremophilane sesquiterpene biosynthesis (Fig. S6A)[20]. The above facts supported the inference that compound **8**, a previously known structure (nigriterpene D[21]) with a double bond at the C6-7 position, might be the precursor of **6**–**7** and certainly **1**, which is characteristic of the aromatic skeleton (Fig. S6B). However, due to the high catalytic activity of JanE, intermediate **8** was consumed rapidly, making it hard to isolate and characterize this product.

To test the above hypothesis, we chemically synthesized compound **8** starting from **6** using the $Mo(CO)_6$-promoted facile dehydrogenation method (Fig. 3B and S183–S190, Table S11, and Supporting Information)[22]. The purified **8** was then fed back into the culture of *Saccharomyces cerevisiae* Y59 expressing the gene *janE* (SC-

Y59-janE). Gratifyingly, compounds **1** (m/z 429 $[2M+H]^+$) and **6** (m/z 249 $[M+H]^+$) (Fig. 3C, iii) were successfully produced, which confirmed ambiguously JanE is responsible for introducing the C6–7 epoxide. However, unexpectedly, the results also indicated that **8** could be transformed into **1** even in the control entry without adding JanE (Fig. 3C, iv), suggesting that a non-enzymic transformation process might take place for **1** formation. Compound **8** was then incubated at 30 °C for 72 h in H_2O (pH 7.0) (Fig. 3D, iv) in a cell-free system. However, the generation of **1** was not observed, which contradicts the result obtained from the non-enzymic transformation experiment. Given that the pH of yeast cultures exhibits dynamic changes during fermentation[23–25], we systematically monitored pH changes in the yeast fermentation system across various cultivation time points (Fig. S7). The experimental data revealed a progressive acidification of the culture medium during metabolism. Based on this observation, we established a pH gradient ranging from 4.0 to 7.0 and subsequently investigated the non-enzymatic transformation of compound **8** in aqueous solutions with varying acidity levels (Fig. 3D). The results revealed that increasing the acidity will significantly enhance the conversion rates from **8** to **1** (Fig. 3D, i–iii). Meanwhile, a byproduct compound **9**, named farfugin C (Fig. 3A, D, Figs. S29–35, and Table S5), was also generated from the acidic environment with pH 4.0. Furthermore, incubating **8** in alkaline gradients also showed improved conversion rates (Fig. S8), which indicated acid–base catalysts may promote the reaction by either increasing the strength of the nucleophile (proton abstraction) and/or the stability of the leaving group (proton donation). The above findings clearly demonstrate two possible biochemical conversion routes for **8**: one pathway involves oxidation catalyzed by JanE to yield epoxide **6** and **7** (Fig. 3A). In contrast, the other pathway entails a non-enzymatic process under acidic or alkaline conditions leading to the formation of aromatic products **1** and **9** (Fig. 3A). During this process, P450 enzyme JanE was identified to be able to introduce the C6–7 double bond and further convert it into an epoxide structure.

Assisted by density functional theory (DFT) calculations, we proposed the detailed conversion steps from **8** to **1** (Fig. 3F, and Fig. S7). For DFT calculation, we adopted two computational methods, M06-2X and B3LYP, both of which are extensively applied in studies on terpene biosynthesis[26–28]. DFT calculations reveal that the reaction proceeds through two critical stages: first, intramolecular cyclization initiated by carbonyl protonation (ΔG = +17.44 kcal/mol), followed by an acid-catalyzed dehydration step (ΔG = +12.79 kcal/mol). Initially, the carbonyl oxygen of compound **8** is protonated by acid, facilitating an intramolecular nucleophilic addition of the lone pair electrons from the C-13 hydroxyl to the C-8 carbonyl, thereby generating a hemiketal intermediate **INT-2R**. The ensuing dehydration at C-8 leads to the formation of the carbocationic intermediate **INT-3**. The calculated activation energy barrier for the dehydration step (+25.6 kcal/mol, Fig. 3D) appears relatively elevated. This may be attributed to the selection of acetic acid (pKa = 4.76) as the acid catalytic model, chosen primarily for simulating the intracellular physiological pH conditions. **INT-3** undergoes two alkyl shifts and dehydrogenation, ultimately yielding **1** (Fig. 3F). The overall reaction pathway bears a resemblance to that observed in the dienone-phenol rearrangement[29], wherein *p*-cyclohexadienone frameworks are converted into phenols (Fig. S9). However, it is noteworthy that product **1** experiences dehydration during this transformation without forming a phenol structure (Fig. 3D). To further investigate and validate the calculated reaction process, we repeated the transformation experiment of compound **8** in a citric acid/Na_2HPO_4 buffer (pH 5) and monitored the reaction mixture using LC–MS asto assess any reaction intermediates. Fortunately, an extra ion peak with m/z 233 $[M+H]^+$, which was attributed to the intermediate of **INT-2R**, was identified from the MS profile (Fig. 3E). However, due to its instability and rapid transformation, we failed to purify **INT-2R**. Nevertheless, the signal intensity of **INT-2R** increased over time as substrate **8** was consumed, providing direct evidence for the involvement of **INT-2R** in the rearrangement process and further supporting the proposed reaction mechanism.

In addition, we successfully isolated and characterized a by-product, compound **9**, which is presumed to be derived from the rearrangement and C4–5 bond cleavage of the carbon cation intermediate **INT-3**, followed by water neutralization of the subsequent carbon cation intermediate of **INT-6**. DFT calculations revealed that the byproduct **9** exhibits a less exergonic reaction profile (ΔG = −36.11 kcal mol^{-1}) compared to the main reaction pathway (ΔG = −56.10 kcal mol^{-1}) (Fig. 3F), indicating its thermodynamic instability relative to compound **1**. These theoretical calculation results align well with the experimental observation that compound **1** was the main product of the rearrangement-aromatic reaction.

Meanwhile, we also tested the effects of acidity and alkalinity on the aromatization reaction of compound **8** by repeating the transformation experiment in different alkaline conditions. Results showed compound **8** could be spontaneously transformed into **1** even in a strong alkaline environment with pH13 (Fig. S8), which aligns with the mechanism wherein deprotonation at the C-13 position is activated under alkaline conditions, thereby facilitating the nucleophilic reaction. In addition, we also tested the progression of the spontaneous transformation of **8** in a broad pH range of 2–16. The results supported the broad pH range for the spontaneous conversions, with the optimal yield achieved at pH 4 (Table S13).

In summary, through in vivo and in vitro transformation experiments and assisted by DFT calculations, we confirmed formation of the aromatic ring is triggered by intramolecular nucleophilic addition of oxygen to carbonyl groups, followed by two [1,2]-methyl shifts and deprotonation to produce **1** (for **9**, only deprotonation is involved). We attributed the core driving force of this kind of reaction to the tendency to form more thermodynamically stable structures with an aromatic ring system. Informed by this mechanism, we also proposed the conversion route for the previously reported citeobenzofuran F[13], which involves a similar nucleophilic addition (Fig. S10).

The flavin-dependent monooxygenase of JanF converts allyl alcohol into α,β-unsaturated aldehyde which serves as the key intermediate of aza-janthinellin A (2a)

Previous experiments demonstrated that the co-expression of *janF* with *janA ~ E* resulted in the disappearance of compounds **1, 6**, and **7** but accumulation of **2a** (Fig. 2B, ii). To further investigate whether **1, 6**, and **7** are precursors responsible for the formation of **2a**, we purified JanF from both *E. coli* and *S. cerevisiae* expression systems and proceeded with in vitro assays using **1, 6**, and **7** as substrates in PBS buffer nourished with L-threonine and FAD. However, multiple attempts failed to produce **2a**. We subsequently repeated the in vitro transformation using the crude enzyme of JanF prepared from cryogenic ground mycelium of the *AN-janF* strain. Results showed that **6** could be completely converted into **2a** after 2 h' incubation, confirming **6** as the precursor of **2a** (Fig. 4A, ii).

Subsequently, to identify the related intermediate participating in the transformation process from **6** to **2a**, we repeated incubating JanF with **6** under different conditions (change of time-course, temperatures, and acidic/basic buffers). The reaction products were then subjected to HPLC and LC–MS analysis to monitor the generation of potential intermediates. Results showed compound **6** was partially consumed in all the entries within the temperature range of 5–45 °C (Fig. S11), however, no final product was detected from the mixture. Subsequently, phylogenic analysis indicated that JanF showed a close evolutionary relationship with MacF[30], which was characterized as a dehydrogenase of the meroterpenoid of macrophorn, AOL_s00251g279[31], proposed to catalyze epoxidation, and HrL4[16], which was responsible for carboxylation of the eremophilane skeleton (Fig. 4A).

https://doi.org/10.1038/s41467-025-62075-4

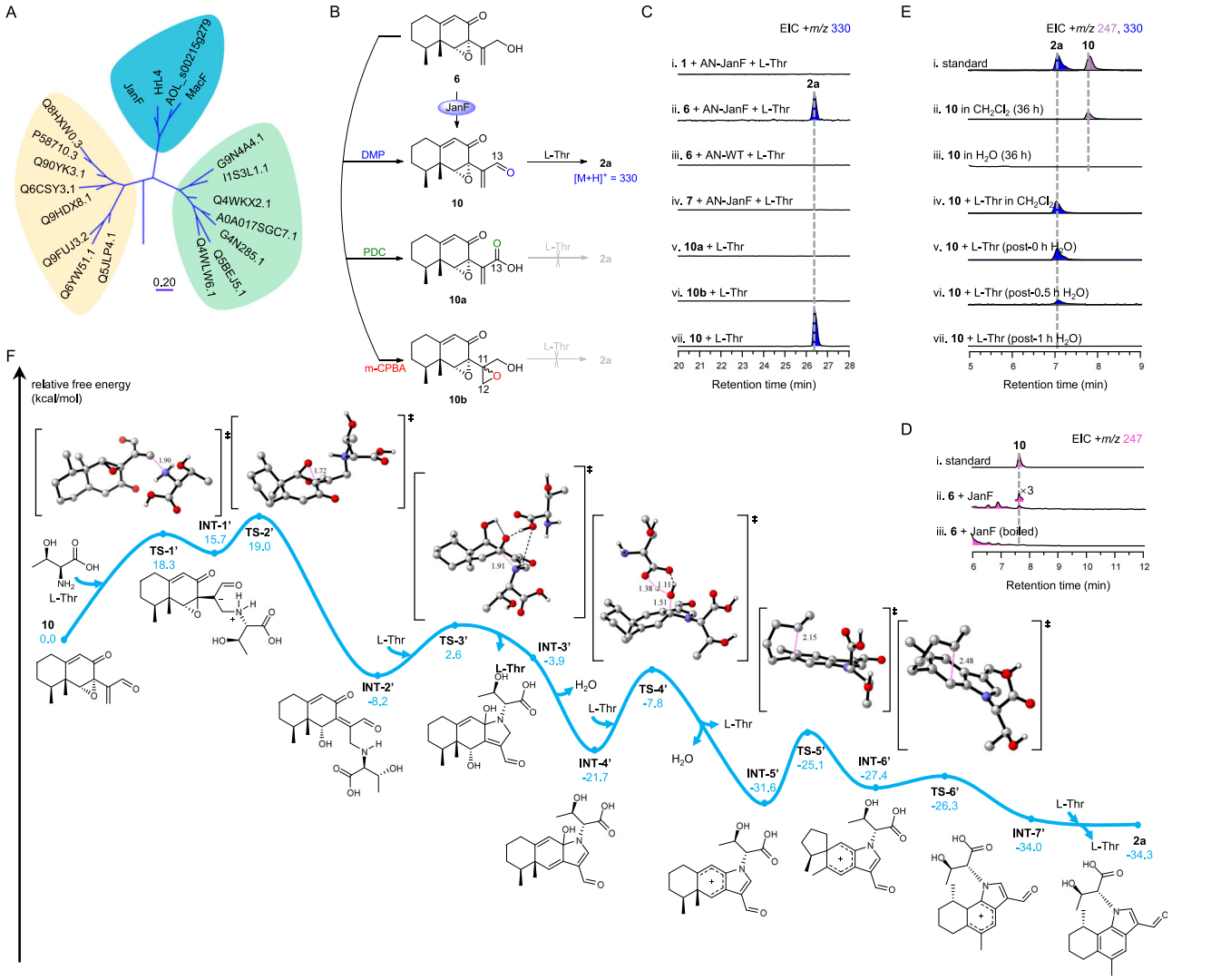

Fig. 4 | Comprehensive analysis of the formation of aza-janthinellin A (2a) triggered by the JanF-mediated aza-Michael addition. A Phylogenetic analysis of JanF with other FMOs from NCBI by the neighbor-joining method using MEGA 11. The bootstrap scores are based on 1000 reiterations. **B** Chemoenzymatic biomimetic simulation of JanF homologs-mediated catalytic transformation of compound **6** (aldehyde/carboxylation/epoxidation-modification) reveals functional characterization of JanF. **C** LC–MS analysis of extracts from in vitro assays involving **1, 6**, and **7** with JanF (i–iv), as well as the incubation of **10a, 10b**, and **10** with L-threonine (v–vii). **D** LC–MS analysis of in vitro reactions of JanF with **6** at 4 °C for 5 min. **E** LC–MS analysis of solvent-dependent stability profiles of compound **10** and its chemoselective conversion with L-Thr, including structural integrity analysis in anhydrous dichloromethane (DCM) vs. aqueous systems (ii–iii), and time-course conversion efficiency correlated with nucleophilic attack mechanisms (iv–vii). **F** Computed energy profile for the proposed nitrogen-binding mechanism from **10** to **2a**. For the 3D structures of **TS-1'**–**TS-6'**, unimportant hydrogens have been omitted for clarity, and bond lengths for partially formed bonds are given in Å (Cartesian coordinates of the optimized structure shown in Supplementary Data 1).

To verify the exact function of JanF (oxygenation or dehydrogenation), we synthesized the aldehyde-derivatized product **10**, the carboxylated product **10a**, and the epoxidized product **10b** using compound **6** as the substrate (Fig. 4B; NMR data for the products are provided in Figs. S182–S201). The incubation experiments showed that only compound **10** could react with L-Thr to form the adduct compound of **2a** (25 °C, 2 h) (Fig. 4C, v–vii), validating the function of JanF as a dehydrogenase that converts the end hydroxyl into an aldehyde. Furthermore, the generation of **10** was detected by LC-MS from the reaction mixture with **6** catalyzed by the crude enzyme of JanF (Fig. 4D), which unambiguously confirmed the function of JanF as an alcohol oxidase.

To gain more insight into the formation of the terpene-amino acid adduct, we then focused on assessing whether the primary amine was bound to **10** before or during the rearrangement process of **10**. For this purpose, we adjusted this reaction process by pre-incubating **10** in water and thereafter added L-threonine to the reaction mixtures with different pre-incubating durations of **10** (Fig. 4E, v–vii). The results still showed the consumption of **10** and generation of **2a** but without any stable intermediate detected from the reaction mixtures. However, with the pre-incubating duration increasing, the production of **2a** decreased accordingly, which means that without the presence of L-threonine, **10** will be consumed and spontaneously converted into unstable intermediates. Moreover, these intermediates are unlikely to react with L-threonine, thus resulting in the production of **2a**. These data suggest the primary amine might be bound to **10** before the spontaneous rearrangement process. We then added L-threonine to the dichloromethane reaction system, where compound **10** could be maintained in a stable state, and the formation of **2a** was consistently observed without any decrease in the final yield of **2a** (Fig. 4E, iv), which also supported the inference above.

Based on the above analysis and assisted by DFT calculations, we propose a nitrogen-binding mechanism for the formation of aza-janthinellin A (**2a**) (Fig. 4F). Due to the strong electron-withdrawing effect of the α,β-unsaturated aldehyde group, the aza-Michael addition of a nucleophilic primary amine to the electrophilic C-12 carbon forms **INT-1'** via the transition state **TS-1'**. Subsequently, the electronic transformation yields the epoxide ring-opened intermediate **INT-2'** via the transition state **TS-2'**. Then the second nucleophilic attack from nitrogen to the C-8 carbonyl produces the tricyclic intermediate, **INT-3'**, via the transition state **TS-3'**, followed by dehydration of the C-8 hydroxyl group, which results in the formation of **INT-4'**. The subsequent steps followed a mechanism analogous to the previously described process of compound **1**, wherein **INT-4'** undergoes two sequential alkyl migrations to yield the stable aromatic structure (Fig. 4F). According to the calculation results, the entire nitrogen-binding reaction is exothermic, with the highest energy barrier of 19.0 kcal/mol, indicating that the process can spontaneously occur at room temperature. As shown in the above reaction scheme, the formation of the aza-aromatic structure of **2a** requires two nucleophilic attacks by nitrogen, while the incubation of **10** with L-threonine would not provide any stable intermediates as analyzed by LC–MS. This may be because the first nucleophilic attack is the rate-limiting step, but once the highly reactive intermediate, such as **INT-2'**, is generated, it is prone to receive a rapid secondary nucleophilic attack at the C-8 carbonyl position to complete the rearrangement-aromatization. In view of this, L-proline, which features a secondary amine instead of a primary amine, was selected as the nucleophile. As proline lacks the second dissociable hydrogen atom, it is not able to promote the second nucleophilic attack, and as a result, further intramolecular cyclization and rearrangement-aromatization will not take place. Under this situation, it would accumulate some enamine intermediate for detection. After incubating **10** and L-proline in water, the imine intermediate of **INT-Pro1** (measured m/z 362.1971, calculated 362.1962, Δ = 0.8831 mmu) and **INT-Pro3** (measured m/z 344.1863, calculated 344.1856, Δ = 2.0499 ppm) were successfully detected (Fig. S13B. C). Based on the above findings, we proposed the reaction cascade for **10** in coupling with L-proline, which includes the following steps: selective nucleophilic attack at C-12, intramolecular cyclization, and dehydration to access the final product (Fig. S13A). The above results further verified the unique ring rearrangement-aromatization mechanism, which requires sequential heteroatom nucleophilic additions as presented in Fig. 4F.

JanF directs regio-selective nucleophilic addition onto the carbonyl group of the α,β-unsaturated ketone-containing substrate

Based on the eremophilane aromatization mechanism proposed above, we hypothesized that the addition of primary amine reagents with strong nucleophilic abilities would facilitate the production of diverse aza-janthinellins. Accordingly, we incubated **6** with a panel of primary amine reagents (1 mg/mL), including ammonia, and amino acids in the presence of JanF. As shown in Fig. 5A, non-native aza-janthinellins B–J (**2b**–**j**) were successfully isolated and characterized from the in vitro conversion results (Figs. S43–S105 and Table S6), thereby confirming the general applicability of the aza-Michael addition in constructing aromatic terpenoid skeletons. The conversion steps starting from **10** and primary amine (e.g., L-glycine) to aza-janthinellins were also supported by DFT calculations (Fig. S14). To determine whether the function of JanF is required in the reaction of **10** with primary amines, we incubated **10** with the above primary amines in buffers with and without the presence of JanF. Consequently, **2b**–**j** were produced in both conditions (Fig. S15). However, in the presence of JanF, the reaction rates of compound **10** with these primary amines were observed to increase to varying extents (Fig. 5B). This indicates that JanF may promote the nucleophilic addition and the aromatization process in the formation of aza-janthinellins. To gain more information regarding the function of JanF in mediating the aza-nucleophilic reactions, we replaced the above primary amines with aniline, which is a relatively weak nucleophilic reagent due to the aniline–allyl conjugation between the nitrogen lone pair and the aromatic system, and repeated the transformation experiments with and without the presence of JanF. In the presence of JanF, the theoretical product **2k** (Figs. S106–S112 and Table S6) was successfully detected (Fig. 5C, ii). In contrast, in the reaction proceeding without JanF, two sesquiterpene-aniline adducts, aza-janthinellins K–L (**2k**–**l**, and S106–S119 and Table S6), were identified (Fig. 5C, iii). This likely occurred because the relatively weak nucleophilicity of the nitrogen decreased its chance in attacking the C-8 ketone group in **10**, but increased the opportunity of dehydration and elimination of the C-6 hydroxyl group, which was possibly derived from the opening of the epoxide caused by the nucleophilic addition of the aniline (Fig. 5D). The dehydration of the **10**-aniline adduct then results in the production of the dienone intermediate **INT-2c'**, which will undergo intramolecular nucleophilic addition in alternative routes: for one route, the nitrogen attacks the α,β-unsaturated ketone at C-8 position (1,2-addition),similar to the case in the formation of **2b**–**j** using alkylamines as stronger nucleophilic reactants (Fig. 4F), and initiates the aromatization process, leading to the production of **2k** (Fig. 5D); for another route, the aza-Michael reaction (1,4-addition) takes place, followed by elimination of the 8-hydroxyl group and subsequent methanolysis to give **2l** (Fig. 5D). To confirm, we re-examined the enzyme-free reaction mixtures of amino acids incubated with **10**. Trace amounts of C-6 addition products **2a'** (*m/z* 347) and **2f'** (*m/z* 393) were detected by LC–MS along with their C-8 addition counterparts (Fig. S16). The above findings verified again that with the presence of JanF, the aza-nucleophilic reaction preferred to take place at the C-8 position.

These results demonstrated that JanF not only functions as a dehydrogenase on the allyl alcohol group on the eremophilane skeleton, but also facilitates the conjugation of eremophilane with primary amines by affecting the regioselectivity during the nucleophilic addition to the α,β-unsaturated ketone intermediate. Using the above logic, we produced a group of aromatic sesquiterpene-amine adducts, greatly expanding the chemical diversity of the aza-janthinellin-like structures.

Studies of catalytic sites and promiscuity of JanF led to the discovery of thio-janthinellins (3) generated by thio-michael addition

Multiple sequence alignment of JanF together with other homologous proteins revealed that JanF conserves His99 as the key residue responsible for covalent binding the cofactor FAD[32], while the sites of Tyr158 and Asn273 are unique to JanF (Fig. S19). To gain insight into the structural basis of the catalytic mechanism of JanF, the 3D structure of JanF was generated through a protein structure prediction service, AlphaFold2[33], and a docking engine AutoDockVina[34], was used to probe the structural details of substrate **6** in binding to JanF (Fig. S17). The results showed that the C-13 atom of **6** was situated 2.9 Å from the N-5 position of the FAD isoalloxazine ring (Fig. 6A). The distances from the C-13 hydroxyl to Tyr158 and from C-8 carbonyl to Asn273 are 3.5 Å and 3.8 Å, which suggests the Tyr158 and Asn273 may stabilize the domain interface by forming a hydrogen bond with the C-8 ketone and C-13 hydroxyl group, thus positioning the substrate correctly (Fig. 6A). To verify the function of these residues, we site-mutated the residues of Tyr158 and Asn273, together with 8 additional residues within 4 Å of **6**. The results demonstrated that, in addition to the H99A mutant, the T158A and N273A mutants also significantly impacted the formation of **2a** (Figs. S18 and 6C, ii and iii). The above bioinformatic analysis and docking-directed site-mutation results supported the inference that His99, Tyr158, and Asn273 are the key sites for the oxidative function of JanF. Among those three residues, His99 acts as the tentacle to attach cofactor FAD, and Tyr158 and Asn273 are responsible for

https://doi.org/10.1038/s41467-025-62075-4

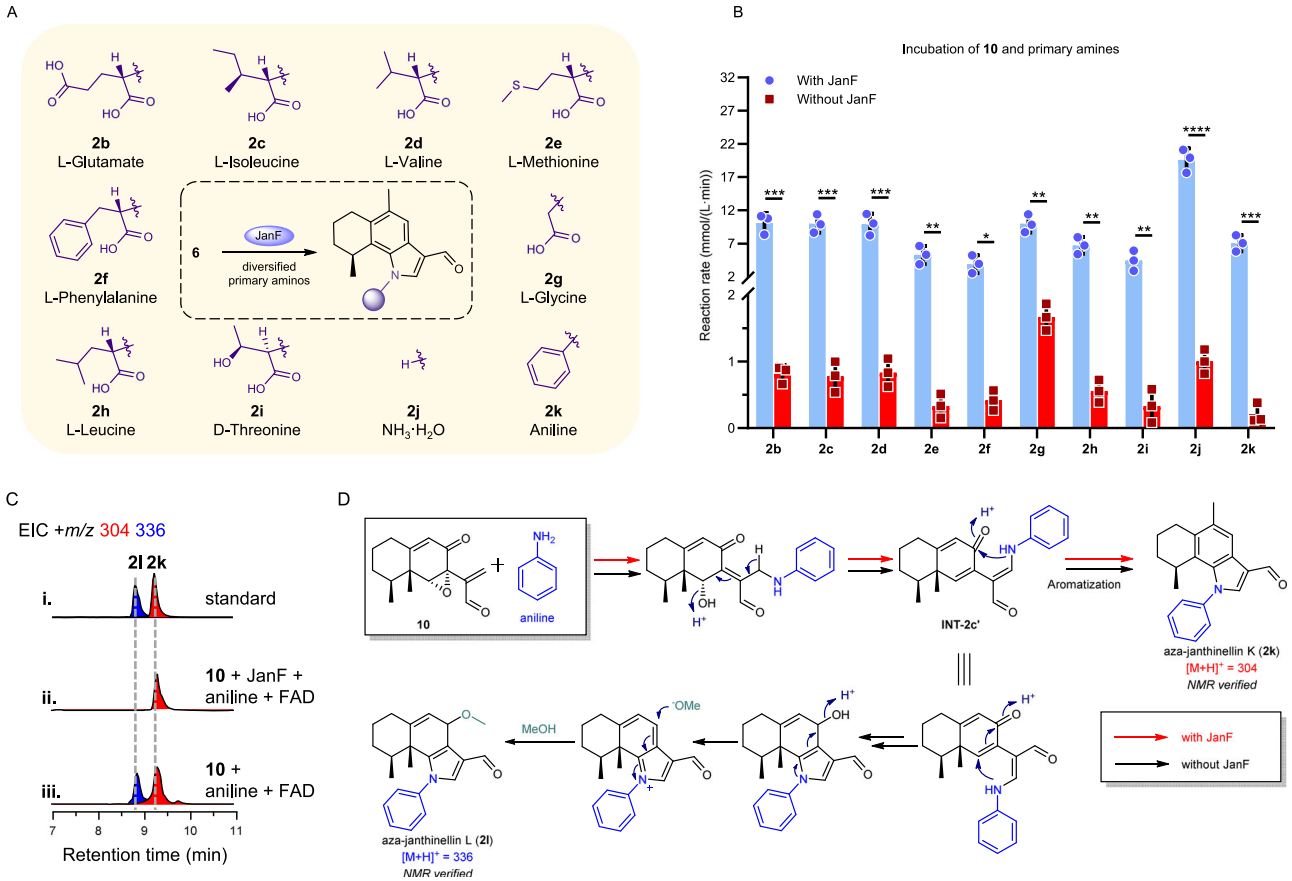

Fig. 5 | Expand the chemical diversity of aza-janthinellins, and molecular docking revealed the spatial selectivity of JanF. A Structure of **2b**–**k**. **B** The comparative analysis of the rates of aza-janthinellins produced in the presence versus absence of JanF. The reactions were carried out as follows: substrate **10** (2 μmol) was mixed at room temperature with amines (2 μmol) in the crude enzyme system (200 μL) of *AN-WT* or *AN-janF* (i.e., with or without JanF present). According to TLC, the time required for the reaction to consume the starting material is calculated, allowing the reaction rates of various primary amines and substrates **10** with and without JanF to be inferred. Data are shown as the mean ± SEM of 3 independent experiments. Analysis used an independent samples *t*-test (two-sided), with no multiple comparison correction, and $p < 0.05$ was defined as statistically significant. $P_{2b} = 0.0005$, $P_{2c} = 0.0003$, $P_{2d} = 0.0006$, $P_{2e} = 0.0034$, $P_{2f} = 0.0113$, $P_{2g} = 0.0004$, $P_{2h} = 0.0011$, $P_{2i} = 0.0100$, $P_{2j} = <0.001$, $P_{2k} = 0.0006$. $^{*}P < 0.05$, $^{**}P < 0.01$, $^{***}P < 0.001$, $^{****}P < 0.0001$. Source data are provided as a Source Data file. **C** LC–MS analysis of extracts from in vitro assays incubating **10** and aniline in the presence and absence of JanF (i–iii). **D** In the presence of JanF, compound **10** was co-incubated with aniline to yield compound **2k**; in the absence of JanF, this reaction also produced compound **2l** alongside compound **2k**.

accommodating and orienting the substrate of **6** in the JanF cavity. Moreover, as reported for other flavn-dependent enzymes[35], the interaction of Tyr158 with the C-13 hydroxyl through a hydrogen bond is important for the efficient hydride ion transfer from the substrate, benefiting the dehydrogenation process.

To better understand the protein-small molecule interaction and the accommodation of these substrates and intermediates, we continued molecular docking studies with JanF and **INT-2c'**, which is a proposed intermediate formed by the addition of aniline to compound **10**. The results indicated that the JanF enzyme cavity has sufficient space to accommodate various aldimine intermediate substrates with a very similar accommodation manner as compound **6**, where Asn273 stabilizes the C-8 carbonyl group via hydrogen bonding, and the aniline moiety in the intermediate is significantly oriented toward the C-8 position. Further molecular docking studies of the enamine intermediates formed between compound **10** and various amino acids revealed that the cavity of JanF has ample space to accommodate a wide range of amino acid substrates (Fig. S20). This protein-substrate interaction effectively explains the preference for the 1,2-addition reaction in the α,β-unsaturated ketone structure. On the one hand, JanF stabilizes the conformation of the enamine intermediate via hydrogen bonds, positioning the nitrogen atom closer to the C-8 carbonyl group in space. On the other hand, Asn273 enhances the electrophilicity of the C-8 position of intermediate **INT-2c'** through hydrogen bonding, thereby facilitating its nucleophilic attack by the nitrogen atom. Subsequently, incubation of compound **10** and aniline in the JanF-N273A variant resulted in the detection of both **2k** and **2l** in the products (Fig. 6C, iv), which confirmed the above mechanism. To further investigate the size of the JanF cavity in accommodation of the enamine intermediates, a large steric hindrance primary amine, amantadine, which bears an adamantanyl substitution, was co-incubated with compound **10**. With the large spatial constraint, adamantylamine is supposed to be unable to enter the cavity of JanF, thus leaving equal reaction opportunities for the C-8 and C-6 nucleophilic attack. To our expectation, the result showed the generation of both the C-8 and C-6 nucleophilic attack products of **2m** and **2m'** (Fig. S21), which was consistent with the results from these JanF-free experiments. The above results strongly support that JanF could accommodate the enamine intermediate with smaller steric hindrance, and meanwhile, composes a regioselectivity effect on the intramolecular nucleophilic attack. Additionally, through site-directed mutagenesis experiments guided by molecular docking analysis combined with in vivo catalytic studies, we confirmed that the sites of Y158 and N273 possibly contribute to binding and stabilizing both the substrate of **6** and the following enamine intermediate such as **INT-2c'** (Fig. 6A, B), thus facilitating the nucleophilic attack at the C-8 position.

https://doi.org/10.1038/s41467-025-62075-4

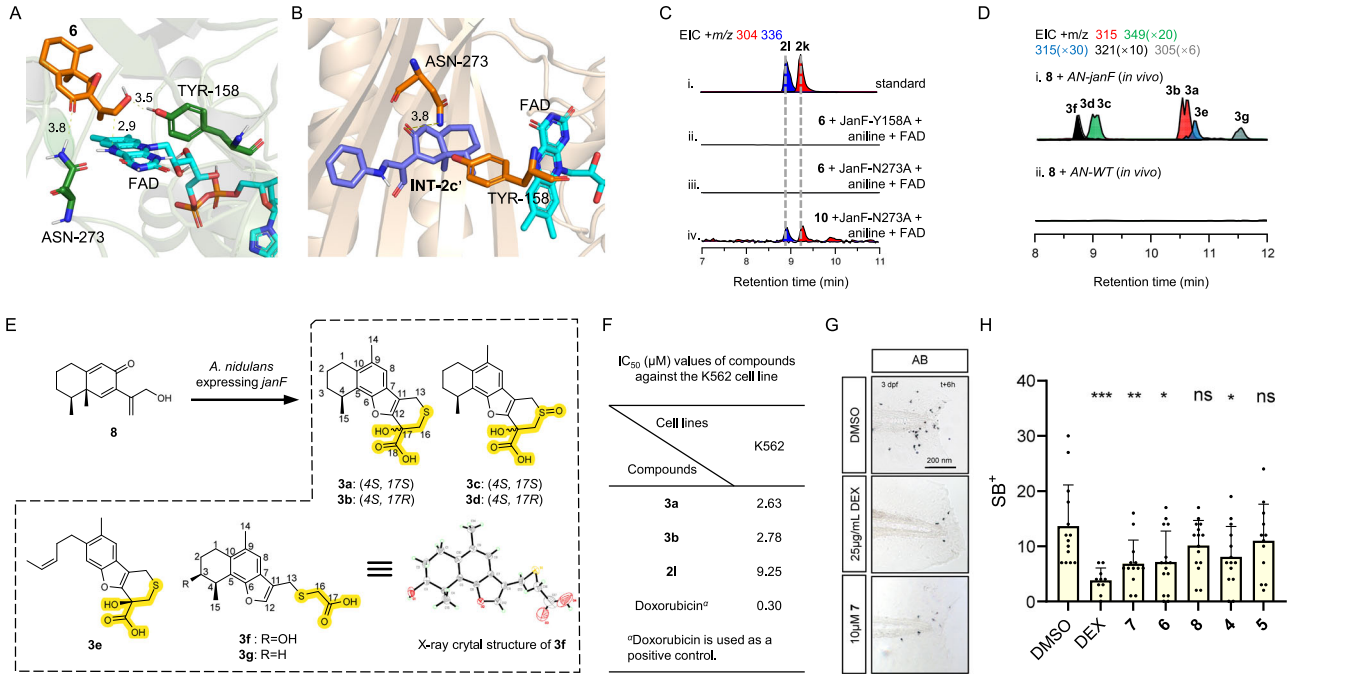

Fig. 6 | Molecular docking revealed the promiscuity of JanF and, based on this, the generation and bioactivity evaluation of thio-janthinellins (3). A JanF active site cavity docked with **6**. Two polar residues of Tyr158 and Asn273 that constitute the substrate binding pocket are indicated (Prompt: without eutectic solutions, docking may not indicate the actual protein-small molecule interactions). **B** Molecular docking revealed the binding mode of the enamine intermediate, which is formed via the condensation of compound **10** with aniline, to the JanF protein. **C** LC–MS analysis of the incubation reactions between aniline and compounds **6** or **10** in the JanF mutant strain. **D 3a** – **g** were produced in the **8**-supplemented cultures of the *AN-janF* transformants. **E 3a** – **g** were produced in the **8**-supplemented cultures of the *AN-janF* transformants. **F** Cytotoxic activity of **3a, 3b**, and **2l**. **G** The black dots are stained with Sudan black and indicate the recruitment number of neutrophils at the injury site of the zebrafish(3dpf) tail fin. Effective compound **7** reduces the number of myeloid cells near the infected tail fin of zebrafish. Source data is provided as a Source Data file. **H** The bar chart is obtained by statistically analyzing the black dots within a 200 nm range from the wound site. Data are shown as the mean ± SEM of 15 independent experiments. The statistical test is Dunnett's multiple comparisons test (two-sided) in the ordinary one-way ANOVA. $P_{DMSO\ vs\ DEX} = 0.0002$, $P_{DMSO\ vs\ 7} = 0.0099$, $P_{DMSO\ vs\ 6} = 0.0106$, $P_{DMSO\ vs\ 8} = 0.3402$, $P_{DMSO\ vs\ 4} = 0.0432$, $P_{DMSO\ vs\ 5} = 0.6771$. * $P < 0.05$, ** $P < 0.01$, *** $P < 0.001$. Source data is provided as a Source Data file.

The molecular docking analyses also indicated that the epoxide group at C6-7 did not interact with JanF, suggesting the catalyzing activity of JanF may be affected little by the modification on such this position and indicating potential promiscuity for JanF. To confirm this inference, we incubated the crude enzyme of JanF with **8**, which possesses a double bond at C6–7 instead of an epoxide. After 12 h-cultivation, we found that **8** was completely consumed but without any products detected, which indicated that some unstable oxidation products were generated, just as the case in the formation of aza-janthinellins. We then added L-threonine to the reaction mixture with the intention of capturing the reactive intermediate. However, there was still no product detected. To determine whether the unstable oxidation product could react with other intracellular metabolites, we repeated in vivo biotransformation in the *AN-janF* living cells. To our delight, the retrieved LC–MS data revealed the emergence of several novel peaks (Fig. 6D, i). After large-scale fermentation, we characterized 7 novel structures designated as thio-janthinellins A–G (**3a**–**g**), all of which are aromatic eremophilane-alkyl thiol adducts (Fig. 6D, E). Their structures with absolute configurations were determined based on extensive NMR spectra and HRESIMS (Figs. S120–S168 and Table S7), ECD calculations (for **3a**, **3b**, and **3e**, Fig. S26), single-crystal X-ray diffraction (for **3f**, CCDC: 2382465), and phenylglycine methyl ester (PGME) transformation (for **3c**/**3d**, Fig. S22, Supporting Information). These structures contain two distinct pairs of diastereomers, **3a**/**3b** and **3c**/**3d**. Among them, the major products, **3a**/**3b**, exhibit an unprecedented pentacyclic meroterpenoid skeleton, comprising a 6/6/5/6 ring system with a rare thiapyran moiety. In contrast, **3c**/**3d** includes a sulfoxide group that is relatively uncommon in NPs. Additionally, compounds **3a**/**3b** were discovered to be able to convert into **3c**/**3d** through gradual oxidation (Fig. S23). Based on the catalytic activity of JanF and the rearrangement mechanism of the cyclohexenone as discovered in the formation of the aza-janthinellins, we proposed a biotransformation pathway leading to the above thio-janthinellins, which required the Michael addition of one molecule of mercaptocarboxylic acid such as β-mercaptopyruvate and thioglycolic acid (commonly found in living cells as a degradation product of cysteine)[36] to one molecule of **8b** in the presence of JanF (Fig. S24), which is responsible for converting the C-13 hydroxyl group into the reactive α,β-unsaturated aldehyde group in **8b**. The conversion from **8b** to **3a**/**3b** was further supported by DFT calculations (Fig. S25). The above results identified a unique methodology for the generation of C-S bonds in constructing novel NP derived skeletons.

Bioactivity evaluation of compounds

The cytotoxicity of **3a, 3b,** and **2l** was evaluated against hthe uman chronic myelogenous leukemia cell line K562 with doxorubicin as a positive control. The results showed that the mono-substituted derivatives displayed moderate to strong cytotoxicity against K562 cells with IC_{50} values ranging from 2.63 to 9.25 μM (Fig. 6F). In addition, the compounds obtained were evaluated for the in vivo anti-inflammatory activity using the zebrafish Tail Amputation Inflammation Model. Wild-type AB line zebrafish were self-bred to obtain eggs, which were immersed in 3% methyl blue solution until 3dpf (3 days post-fertilization). Then, the wild-type AB strain zebrafish larvae of 3dpf were anaesthetized with 0.2% tricaine solution, and the caudal fin was truncated using a sterile 1 mL syringe needle to establish the Tail Amputation Inflammation Model. Results showed that compound **7** could reduce adjacent myeloid cells near the infected caudal fin, which

was comparable to the positive control dexamethasone (Fig. 6G, H). The thio-containing compounds were also tested for their antibacterial activity against a panel of Gram-negative and Gram-positive pathogens. As a result, compounds **3a** and **3c** showed promising activity against the Gram-negative pathogen of *Acinetobacter baumannii* AB34 with MICs of 32 μM and 16 μM, and compounds **3f** and **3g** showed activity against the Gram-positive pathogen of *Staphylococcus aureus* with MICs of 16 μM and 32 μM, respectively (Table S14).

Discussion

By reconstituting an isoprenoid biosynthetic pathway in *A. nidulans*, we successfully obtained a series of eremophilane derivatives, among which farfugin A (**1**) and aza-janthinellin A (**2a**) feature intriguing aromatic skeletons derived from the aristolochene skeleton. Notably, the discovery of **2a** has put forward an NP resource of azaphilic structures originating from the isoprenoid pathway, in addition to the well-known azaphilonoids derived from polyketide biosynthetic pathways.

Biosynthetic studies of those aromatic terpenoid structures have unraveled an unprecedented type of aromatization mechanism which involves two consecutive [1,2]-alkyl migrations initiated by intramolecular spontaneous oxo-/aza-nucleophilic addition. During this process, a group of oxygenases (P450s of JanB, D, E, SDR of JanC, and FMO of JanF) play crucial roles in modifying the aristolochene skeleton and providing highly reactive intermediates. Among these enzymes, JanF mediates the formation of **2a** by oxidizing α,β-unsaturated alcohols to α,β-unsaturated aldehydes. The aza-nucleophilic promoted aromatization reaction involved in the formation of **2a** demonstrates a feasible method for constructing cyclohexylindole skeletons by adding primary amine building blocks to a sesquiterpene framework.

Inspired by the afore-mentioned mechanism, we established a cell-free biotransformation system that incorporated phomenone B (**6**) and amino acids as precursors, utilizing JanF's FMO as the catalyst. This system supports the generation of a series of sesquiterpene-amine adducts. When phomenone B (**6**) was substituted with nigriterpene D (**8**) in the reaction system, several sesquiterpene-mercaptocarboxylic acid adducts (**3**) were generated, confirming JanF's promiscuity in catalyzing the dehydrogenation of eremophilane substrates. Notably, compounds **3a** and **3b** exhibited remarkable cytotoxicity against the K562 cell line, thereby validating the feasibility of leveraging the substrate promiscuity of this biotransformation system to generate bioactive compounds for drug discovery and development.

In conclusion, this report elucidates an unusual machinery for the biosynthesis of a group of aromatic sesquiterpenoids, which involves several enzymatic and non-enzymatic steps emphasized by rearrangement of the sesquiterpenoid skeleton, which was initiated by heteroatom nucleophilic addition in the biosynthesis of a group of aromatic sesquiterpenoids. This innovative biosynthetic logic has enhanced our understanding of the biogenesis of aromatic compounds and provides a route to construct aza- and thio-containing terpenoids with expanded diversity and biological activity.

Methods

General experimental procedures

Specific rotations were obtained on a JASCO P-1020 digital polarimeter. UV spectra were recorded from 200 to 600 nm on a Hitachi 5430. ECD spectra were measured on a JASCO J-715 spectropolarimeter. NMR spectra were recorded on Agilent 500 MHz DD2 spectrometers (Agilent, Beijing, China) using tetramethylsilane as an internal standard, and the chemical shifts were recorded in δ values. HRESIMS were obtained using a Thermo Scientific LTQ Orbitrap XL mass spectrometer. Semipreparative HPLC was performed using an ODS column [HPLC (YMC-Pack ODS-A, 10 × 250 mm, 5 μm, 3 mL/min)]. High-performance liquid chromatography–ultraviolet–mass spectrometry (LC–UV–MS) was performed on a Waters SQ Detector Liquid mass spectrometer (USA) using Waters ACQUITY UPLC Shield RP18 (1.7 μm, 21 × 50 mm, 0.5 mL/min). Column chromatography (CC) was performed with silica gel (100–200 mesh, 200–300 mesh, Qingdao Marine Chemical Inc.) and Sephadex LH-20 (Amersham Biosciences), respectively. UV spectrum of DNA was recorded on a NP80 NanoPhotometer (Implen) with an 8.5 mm cuvette. All chemicals used in the study were of analytical grade, except the preparative HPLC and LC–MS, with chromatographic grade.

General DNA manipulation techniques

All the DNA manipulations in this study were conducted according to the manufacturer's protocol. PCR reactions were performed using the Phusion® high-fidelity DNA polymerase, Q5® High-Fidelity DNA Polymerases (New England Biolabs), Hieff Canace® Gold High-Fidelity DNA Polymerase (Yeasen), and KOD OneTM PCR Master Mix (Toyobo) according to the manufacturer's instructions. cDNA was synthesized by using the PrimeScript RT-PCR Kit (TaKaRa). Custom oligonucleotides were synthesized by Shanghai Sangon DNA Technologies. Fragments were respectively amplified by the condition: step 1: 95 °C for 3 min; step 2: 95 °C for 15 s; step 3: Tm for 15 s; step 4: 72 °C by 30 s/kb (KOD for 5 s/kb); step 5: step 2 to step 4 for 35 cycles; step 6: 72 °C 10 min, then the products were purified by gel. *Escherichia coli strain* XL-1 was used for routine cloning. *Saccharomyces cerevisiae* Y31 was used for in vivo yeast DNA recombination cloning. *Saccharomyces cerevisiae* Y59 was used to express target enzymes and cultured on yeast extract peptone dextrose (YPD) medium at 28 °C for microsomal in vitro assays. *Penicillium janthinellum* H7-4 was cultured at 28 °C on PDA plates, and spores were collected after 7 days of growth by flooding the plates with sterile 0.1% Tween 80. H7-4 was grown in Elenmeyer flasks containing 150 mL of liquid culture medium, composed of glucose (1%), maltose (2%), mannitol (2%), monosodium glutamate (1%), KH_2PO_4 (0.05%), $MgSO_4{\cdot}7H_2O$ (0.03%), and yeast extract (0.3%) after adjusting its pH to 6.5 before RNA isolation or in PDA medium for isolation of genomic DNA. *Aspergillus nidulans* A1145 was grown at 28 °C in CD (0.1% Glucose, 0.5 v/v% 20× nitrate salts, 0.01 v/v% trace elements, and 2% agar for solid media) media for sporulation or in CD-ST (2% starch, 2% casamino acids, 5 v/v% 20×nitrate salts, 0.1 v/v% trace elements) media for heterologous expression and compound production.

Heterologous expression of *jan* gene cluster in *Aspergillus nidulans*

The *jan* gene cluster sequences were PCR-amplified using genomic DNA from *Penicillium janthinellum* H7-4 as a template, with primer sequences detailed in Table S3. For vector preparation, plasmids pYTU (pyrG), pYTP (pyroA), and pYTR (riboB)—carrying auxotrophic markers for uracil, pyridoxine, and riboflavin biosynthesis, respectively—were digested with PacI and SwaI restriction enzymes. The resulting fragments were used in yeast homologous recombination to construct heterologous expression plasmids. Colonies confirmed by PCR were pooled, and the plasmids were extracted using a yeast miniprep protocol. Purified plasmids were then transformed into *Escherichia coli* XL-1 cells via electroporation using the Zyppy Plasmid Miniprep Kit (Zymo Research, USA). Single-plasmid transformants were identified through bacterial plasmid isolation and verified by DNA sequencing before being cataloged as recombinant plasmids (Table S2). For transformation of *Aspergillus nidulans* strain A1145, 50 μL of freshly prepared protoplast suspension was mixed with the target plasmids and incubated on ice for 60 minutes. Following this, 500 μL of PEG solution (60% PEG, 50 mM $CaCl_2$, 50 mM Tris-HCl, pH 7.5) was added, and the mixture was incubated at room temperature for 20 minutes. The transformation mixture was then spread onto regeneration medium consisting of CD agar supplemented with 1.2 M sorbitol and appropriate nutrients (10 mM uridine, 5 mM uracil, 0.5 μg/mL pyridoxine HCl, and/or 2.5 μg/mL riboflavin, depending on the plasmid

selection marker). After incubation at 37 °C for 2–3 days, individual colonies were transferred to CD-ST liquid medium (composition per liter: 20 g starch, 20 g tryptone, 50 mL 20× nitrate salts, 1 mL trace elements, pH 6.5) for metabolite production.

Biotransformation assays with microsomal *S. cerevisiae*

To verify the function of enzyme(s) of interest by yeast biotransformation, the *S. cerevisiae* Y59 strain transformed with individual plasmids was used for biotransformation. The transformant yeast strains were selected on solid selective drop-out media for 2–3 days, then single colonies were inoculated into 3 mL selective drop-out media and grown for 24 h to be used as inocula for YPD media. The yeast microsomes or crude enzymes were then extracted and co-incubated with different substrates as described earlier. The products of different reaction systems were analyzed and detected by LC–MS to judge the reaction situations (spontaneous reaction verification experiments based on H^+ were added in different time intervals of different reaction systems according to requirements).

In vitro assay for JanE

For in vitro assays of JanE, centrifugation of yeast overexpressing JanE (25 mL at 28 °C, 250 g for 3 days in YPD medium) was performed and submerged in liquid nitrogen, and then resuspended in buffer C. The crude enzyme was incubated with different substrates and cofactors: 20 μM **8**, 400 μM NADPH in a total 100 μL reaction. The reaction was incubated at 28 °C overnight and extracted with 100 μL ethyl acetate twice. After the solvent was evaporated, the extraction of this system was dissolved in methanol and detected by HPLC.

Spontaneous reactions of 8

For determining the pH effects on the reactions, assays were performed in a total volume of 100 μL containing 100 μM **8**, in H_2O with pH values ranging from 4 to 7, with incubation at 30 °C for 72 h. The buffers were prepared as follows: citric acid/Na_2HPO_4 buffer (pH 4–6); H_2O (pH 7). In general, the reactions were analyzed by HPLC using the general analytical HPLC method.

Biotransformation assays with the crude enzyme of *A. nidulans*

To verify the function of enzyme(s) of interest by *A. nidulans* biotransformation, the *A. nidulans* A1145 strain transformed with individual plasmids was used for biotransformation. The transformant strains were selected on solid selective drop-out media for 2–3 days, then single colonies were inoculated into 20 mL selective drop-out media and grown for 3 days to be used as inocula in CD-ST medium. The crude enzymes were then extracted and co-incubated with different substrates as described earlier. The products of different reaction systems were analyzed and detected by LC–MS to judge the reaction situation.

In vitro assay for JanF

For in vitro assays of JanF, centrifugation of *A. nidulans* A1145 overexpressing JanF (25 mL at 28 °C, 250 g for 3 days in CD-ST medium) was performed and submerged in liquid nitrogen, and then resuspended in buffer C. The crude enzyme was incubated with different substrates and cofactors: 20 μM **1, 6,** and **7**, 20 μM FAD in a total of 100 μL reaction. The reaction was incubated at 28 °C overnight and extracted with 100 μL ethyl acetate twice. After the solvent was evaporated, the extraction of this system was dissolved in methanol and detected by HPLC.

In vitro assay for JanF$^{H99A/Y158A/N273A/S275A/T277A/F334A/F343A/T382A/T384A/L417A}$

For in vitro assays of JanF$^{H99A/Y158A/N273A/S275A/T277A/F334A/F343A/T382A/T384A/L417A}$, centrifugation of *A. nidulans* A1145 overexpressing JanF site-directed mutants (25 mL at 28 °C, 250 g for 3 days in CD-ST medium) was performed and submerged in liquid nitrogen, and then resuspended in buffer C. The crude enzyme was incubated with different substrates and cofactors: 20 μM **6**, 20 μM FAD, and 20 μM L-Thr in a total 100 μL reaction. The reaction was incubated at 28 °C overnight and extracted with 100 μL ethyl acetate twice. After the solvent was evaporated, the extraction of this system was dissolved in methanol and detected by HPLC.

Feeding experiments using the *AN-janF*

For feeding experiments in *A. nidulans*, **8** (1 mg) was added to 100 mL of CDST medium, 2 days after the cultivation of the *AN-JanF* transformants. After further incubation at 28 °C for 2 days, the fermentation broth was extracted with ethyl acetate twice and concentrated in vacuo. The dried extracts were dissolved in methanol for HPLC analysis.

Spontaneous reaction of compound 10 with primary amines

A typical reaction mixture included 100 μM **10** and 200 μM L-Thr in H_2O in a total volume of 100 μL with incubation at 30 °C for 2 h. Products were analyzed by HPLC using the general analytical HPLC method or subjected to LC–MS analysis.

Commonly misidentified lines

K562 cells are frequently misidentified as HL-60 cells in experimental settings due to overlapping morphological and functional characteristics. Nevertheless, K562 cells serve a critical and irreplaceable function in chronic myeloid leukemia-targeted therapy, immunotherapy, and high-throughput drug screening, offering robust and reliable biological support for experimental outcomes.

Reporting summary

Further information on research design is available in the Nature Portfolio Reporting Summary linked to this article.

Data availability

The data supporting the conclusions of this study are presented in the main text, Supplementary Information, and from the corresponding author upon request. Source data are provided with this paper. The X-ray crystallographic coordinates for structures reported in this study have been deposited at the Cambridge Crystallographic Data Centre (CCDC), under deposition numbers 2341504 [https://doi.org/10.5517/ccdc.csd.cc2jljd2], 2341506 [https://doi.org/10.5517/ccdc.csd.cc2jljg4], and 2382465 [https://doi.org/10.5517/ccdc.csd.cc2kz4qf]. These data can be obtained free of charge from The Cambridge Crystallographic Data Centre via www.ccdc.cam.ac.uk/data_request/cif. Source data are provided with this paper.

References

1. Maeda, H. & Dudareva, N. The shikimate pathway and aromatic amino Acid biosynthesis in plants. *Annu. Rev. Plant Biol.* **63**, 73–105 (2012).
2. Larsen, E. M., Wilson, M. R. & Taylor, R. E. Conformation-activity relationships of polyketide natural products. *Nat. Prod. Rep.* **32**, 1183–1206 (2015).
3. Pham, J. V. et al. A review of the microbial production of bioactive natural products and biologics. *Front. Microbiol.* **10**, 1404 (2019).
4. Huang, J. Q. et al. Aromatization of natural products by a specialized detoxification enzyme. *Nat. Chem. Biol.* **16**, 250–256 (2020).
5. Wang, G. Q. et al. Biosynthetic pathway for furanosteroid demethoxyviridin and identification of an unusual pregnane side-chain cleavage. *Nat. Commun.* **9**, 1838 (2018).
6. Yuyama, K. T., Fortkamp, D. & Abraham, W. R. Eremophilane-type sesquiterpenes from fungi and their medicinal potential. *J. Biol. Chem.* **399**, 13–28 (2018).

7. Hou, C., Kulka, M., Zhang, J., Li, Y. & Guo, F. Occurrence and biological activities of eremophilane-type sesquiterpenes. *Mini Rev. Med. Chem.* **14**, 664–677 (2014).
8. Moule, Y., Jemmali, M. & Rousseau, N. Mechanism of the inhibition of transcription by pr toxin, a mycotoxin from *Penicillium roqueforti*. *Chem. Biol. Interact.* **14**, 207–216 (1976).
9. Huang, Y. F., Qiao, L., Lv, A. L., Pei, Y. H. & Tian, L. Eremophilane sesquiterenes from the marine fungus *Penicillium* sp. BL27-2. *Chin. Chem. Lett.* **19**, 562–564 (2008).
10. Cane, D. E. & Kang, I. Aristolochene synthase: purification, molecular cloning, high-level expression in *Escherichia coli*, and characterization of the *Aspergillus terreus* cyclase. *Arch. Biochem. Biophys.* **376**, 354–364 (2000).
11. Hidalgo, P. I. et al. Molecular characterization of the PR-toxin gene cluster in *Penicillium roqueforti* and *Penicillium chrysogenum*: cross talk of secondary metabolite pathways. *Fungal Genet. Biol.* **62**, 11–24 (2014).
12. Nakashima, K. I. et al. Paraconiothins A-J: sesquiterpenoids from the endophytic fungus *Paraconiothyrium brasiliense* ECN258. *J. Nat. Prod.* **82**, 3347–3356 (2019).
13. Wu, Q. et al. Citreobenzofuran D–F and phomenone A-B: five novel sesquiterpenoids from the mangrove-derived fungus *Penicillium* sp. HDN13-494. *Mar. Drugs* **20**, 137 (2022).
14. Nagano, H. et al. Farfugin A and B, new sesquiterpenes from *Farfugium japonicum*. *ChemInform* **4**, 197294611 (1973).
15. Hidalgo, P. I. et al. *Penicillium roqueforti* PR toxin gene cluster characterization. *Appl. Microbiol. Biotechnol.* **101**, 2043–2056 (2017).
16. Sun, Y. et al. Rapid discovery of terpene tailoring enzymes for total biosynthesis. *Chem. Sci.* **14**, 13463–13467 (2023).
17. Chiang, Y. M. et al. An efficient system for heterologous expression of secondary metabolite genes in *Aspergillus nidulans*. *J. Am. Chem. Soc.* **135**, 7720–7731 (2013).
18. Daengrot, C. et al. Eremophilane sesquiterpenes and diphenyl thioethers from the soil fungus *Penicillium copticola* PSU-RSPG138. *J. Nat. Prod.* **78**, 615–622 (2015).
19. Saito, Y. et al. Four new eremophilane-type alcohols from *Cremanthodium helianthus* collected in China. *Nat. Prod. Commun.* **7**, 423–426 (2012).
20. Sato, Y. et al. Bioinformatics-guided reconstitution of biosynthetic machineries of fungal eremophilane sesquiterpenes. *ACS Chem. Biol.* **19**, 861–865 (2024).
21. Chang, J. C. et al. Bioactive constituents from the termite nest-derived medicinal fungus *Xylaria nigripes*. *J. Nat. Prod.* **80**, 38–44 (2017).
22. Patra, A., Bandyopadhyay, M. & Mal, D. Mo(CO)6-promoted facile deoxygenation of α,β-epoxy ketones and α,β-epoxy esters. *Tetrahedron Lett.* **44**, 2355–2357 (2003).
23. Feng, C. A. O. et al. Analysis of intracellular metabolism of *Saccharomyces cerevisiae* in logarithmic growth stage. *Food Ferment. Ind.* **48**, 68–75 (2022).
24. Kawahata, M., Masaki, K., Fujii, T. & Iefuji, H. Yeast genes involved in response to lactic acid and acetic acid: acidic conditions caused by the organic acids in *Saccharomyces cerevisiae* cultures induce expression of intracellular metal metabolism genes regulated by Aft1p. *FEMS Yeast Res.* **6**, 924–936 (2006).
25. Chidi, B. S., Bauer, F. F. & Rossouw, D. Organic acid metabolism and the impact of fermentation practices on wine acidity: a review. *S. Afr. J. Enol. Vitic.* **39**, 2 (2018).
26. Zhao, Y. & Truhlar, D. G. The M06 suite of density functionals for main group thermochemistry, thermochemical kinetics, noncovalent interactions, excited states, and transition elements: two new functionals and systematic testing of four M06-class functionals and 12 other functionals. *Theor. Chem. Acc.* **120**, 215–224 (2008).
27. Stephens, P. J., Devlin, F. J., Chabalowski, C. F. & Frisch, M. J. Ab initio calculation of vibrational absorption and circular dichroism spectra using density functional force fields. *J. Phys. Chem.* **98**, 11623 (1994).
28. Takeshi, Y., David, P. T. & Nicholas, C. H. A new hybrid exchange–correlation functional using the Coulomb-attenuating method (CAM-B3LYP). *Chem. Phys. Lett.* **393**, 51–57 (2004).
29. Li, J. J. *Name Reactions. A Collection of Detailed Mechanisms and Synthetic Applications*. (Springer, Berlin, Heidelberg, 2009).
30. Tang, M. C. et al. Late-stage terpene cyclization by an integral membrane cyclase in the biosynthesis of isoprenoid epoxycyclohexenone natural products. *Org. Lett.* **19**, 5376–5379 (2017).
31. He, Z. Q. et al. Polyketide synthase-terpenoid synthase hybrid pathway regulation of trap formation through ammonia metabolism controls soil colonization of predominant nematode-trapping fungus. *J. Agric. Food Chem.* **69**, 4464–4479 (2021).
32. Paul, C. E. et al. Flavoprotein monooxygenases: versatile biocatalysts. *Biotechnol. Adv.* **51**, 107712 (2021).
33. Jumper, J. et al. Highly accurate protein structure prediction with AlphaFold. *Nature* **596**, 583–589 (2021).
34. Eberhardt, J., Santos-Martins, D., Tillack, A. F. & Forli, S. AutoDock Vina 1.2.0: New docking methods, expanded force field, and Python bindings. *J. Chem. Inf. Model.* **61**, 3891–3898 (2021).
35. Yuan, H. & Gadda, G. Importance of a serine proximal to the C(4a) and N(5) flavin atoms for hydride transfer in choline oxidase. *Biochemistry* **50**, 770–779 (2011).
36. Shatalin, K., Shatalina, E., Mironov, A. & Nudler, E. H_2S: a universal defense against antibiotics in bacteria. *Science* **334**, 986–990 (2011).

Acknowledgements

This research was funded by Qingdao Marine Science and Technology Center (2022QNLM030003-2 to G.Z.), the National Natural Science Foundation of China (32370061 to G.Z.), Taishan Scholar Youth Expert Program in Shandong Province (tsqn 202103153 to G.Z.), Major Basic Research Programs of Natural Science Foundation of Shandong Province (ZR2023ZD29 to G.Z.), Hainan Provincial Joint Project of Sanya Yazhou Bay Science and Technology City (2021CXLH0012 to T.Z.), the team project of "Subject Enrichment, Innovation and Quality Improvement" in Guangdong Pharmaceutical University (No. 2024ZZ08 to J.S). The authors thank Prof. Yi Tang from the University of California for donating the heterologous expression plasmids and strains.

Author contributions

G.Z. performed the project conception and administration, funding acquisition, and manuscript review and editing. H.X. performed the data curation and formal analysis with all bioinformatics analysis, plasmid construction, heterologous expression, compound isolation and characterization, in vivo and in vitro biochemical experiments, and organic synthesis. Y.C. conducted most computational studies. X.H. analyzed the structures of compounds. K.Z. and C.M. performed the validation of data and guidance on molecular biology experiments. R.F. and J.S. performed an anti-inflammatory activity experiment. X.Z., Y.Z., G.L., and X.L. performed PCR of gene fragments and verification of mutants. B.P. guided the experiment and revised the paper. Q.C. and T.Z. checked the procedures of this work.

Competing interests

The authors declare no competing interests.

Additional information

Supplementary information The online version contains supplementary material available at https://doi.org/10.1038/s41467-025-62075-4.

Correspondence and requests for materials should be addressed to Guojian Zhang.

Peer review information *Nature Communications* thanks the anonymous reviewer(s) for their contribution to the peer review of this work. A peer review file is available.